Gbit/s-operation of graphene electro-absorption modulators in a passive polymer waveguide platform for data and telecommunications

M. Kleinert*[a], P. Reinke[a], H.-G. Bach[a], W. Brinker[a], C. Zawadzki[a], A. Dietrich[a], D. de Felipe[a], N. Keil[a], M. Schell[a]
[a]Fraunhofer Heinrich Hertz Institute, Einsteinufer 37, 10587 Berlin, Germany

ABSTRACT

Graphene with its high carrier mobility as well as its tunable light absorption is an attractive active material for high-speed electro-absorption modulators (EAMs). Large-area CVD-grown graphene monolayers can be transferred onto arbitrary substrates to add active optoelectronic properties to intrinsically passive photonic integration platforms.

In this work, we present graphene-based EAMs integrated in passive polymer waveguides. To facilitate modulation frequencies in the GHz range, a 50 Ω termination resistor and a DC blocking capacitor are integrated with graphene EAMs for the first time.

Large signal data transmission experiments were carried out across the O, C and L optical communications bands. The fastest devices exhibit a 3-dB bandwidth of more than 4 GHz. Our analytical model of the modulation response for the graphene-based EAMs is in good agreement with the measurement results. It predicts that bandwidths greater than 50 GHz are possible with future device iterations.

Owing to the absorption properties of the graphene layers, the devices are expected to be functional at smaller wavelengths of interest for optical interconnects and data communications as well, offering a novel flexibility for the integration of high-speed functionalities in optoelectronic integrated circuits. Our work is the first step towards an Active Optical Printed Circuit Board, hiding the optics completely inside the board and thus removing entry barriers in manufacturing. We believe this will lead to the same success as observed in Active Optical Cables for short range optically wired connections.

Keywords: Graphene, electro-absorption modulator, integrated optics, active optical printed circuit board, polymer waveguides

1. INTRODUCTION

The amount of data transmitted in the worldwide telecommunications networks continues to increase with a push towards higher bandwidths to the households using FTTx schemes. It is even eclipsed by the growth of the bandwidth demand within data centers, especially driven by cloud computing and video-on-demand. As both FTTx and datacenter applications are especially cost sensitive new optoelectronic device concepts that can deliver high bandwidths at reasonable costs are needed.

Monolithic integration of optoelectronic functionalities in semiconductor-based material systems such as InP and silicon-on-insulator is able to achieve a great degree of functionality on a single die [1, 2]. However, this complexity comes along with chip costs that may prevent a lot of applications. The hybrid integration of electro-optically active and passive material systems has been proven to be a promising way to obtain photonic integrated circuits (PICs) with a similar level of functionality at potentially lower prices. Prominent hybrid integrated platforms are the TriPleX platform based on silicon nitride waveguides [3] and HHI's passive polymer waveguide platform PolyBoard [4].

While laser diodes and photodetectors can easily be coupled to either end of passive waveguide network in order to accomplish hybrid integration, the flexible integration of high-speed modulators remains challenging due to the large number of waveguide coupling points and the separation of the passive wave-guiding structure into at least two separate dies. Hence, the flexible integration of modulation capabilities into intrinsically passive waveguides is an attractive feature for the further development of low-cost optoelectronic devices for data and telecommunications.

*moritz.kleinert@hhi.fraunhofer.de; phone +49 30 31002-380; hhi.fraunhofer.de

Due to its unique mechanical, optical and electrical properties, graphene is a promising candidate for this objective. Being a monolayer of carbon atoms with a thickness of mere 0.35 nm, it can almost seamlessly be integrated into existing waveguide layer structures. The linear energy dispersion relation leads to an optical absorption in the graphene layer that is tunable with an external voltage and to electrical charge carriers with almost vanishing effective mass. This combination enables the realization of waveguide integrated graphene-polymer electro-absorption modulators (EAMs), where the carrier-induced bandwidth limitation is in the order of some hundreds of GHz or even up into the THz range.

Such EAMs were demonstrated in silicon and polymer waveguide networks in previous work [5–10]. For non-resonant structures, the highest reported bandwidth is 35 GHz by *Dalir et al* [10]. This was achieved by decreasing the capacitance of the EAM section by using a 120 nm thick Al_2O_3 layer. However, this comes at the expense of unpractically high modulation voltages of 25 V. *Liu et al.* demonstrated optoelectronic bandwidths of up to 1.2 GHz at moderate modulation voltages of 3.5 V [5]. The bandwidth limitation for all published graphene-based EAMs is the RC constant of the capacitor structures. Although graphene features a high carrier mobility and a high specific conductivity, the sheer thinness of the atomic monolayer results in comparatively high sheet resistances in the order of 400 Ω/□ to 600 Ω/□ [11]. This translates to a non-negligible contribution to the series resistance of the devices. Furthermore, the tuning of graphene's Fermi level in EAM structures necessary for optical modulation requires the induction of carrier densities in capacitor structures. For standard data and telecommunications wavelengths in the near infrared, reasonable modulation voltages of some volts require capacitors with some tens of nanometers spacing, resulting in high capacitances. This is the reason for the apparent discrepancy between the theoretically possible device bandwidths and the practically achievable ones.

This almost pure RC limitation of the bandwidth makes the careful co-development of electronic and optoelectronic aspects of graphene-based EAMs necessary. In this work, we demonstrate the integration of such EAMs with a 50 Ω termination resistance, a blocking capacitor as well as a 50 Ω impedance matched electrical transmission line for the first time. The first part of this paper deals with the design considerations of such devices, followed by the fabrication and characterization. Finally, the implications on further developments will be discussed.

2. DESIGN AND SIMULATION OF GRAPHENE EAMS

2.1 Optical design and simulations

The devices presented in this work feature an active region consisting of graphene-polymer waveguide integrated electro-absorption modulators (GP-EAMs) with a cross section as shown in Figure 1.

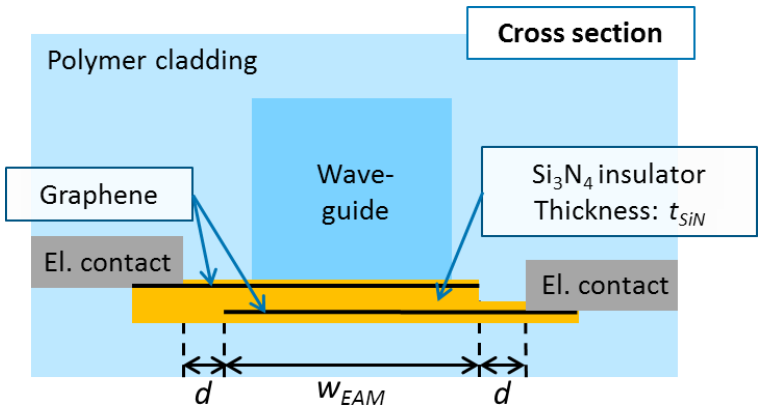

Figure 1. Sketch (not to scale) of the waveguide cross section inside the active region of the GP-EAM.

The embedding of the graphene layers below the waveguide enables the transfer of the graphene layers to smooth unstructured surfaces, minimizing the risk of tearing during the transfer process und thus increasing the device yield. The upper and lower graphene layers are insulated by 50 nm silicon nitride and covered by 10 nm silicon nitride above and below. In this way, a symmetric structure is achieved, which is important for a proper device operation. The refractive index n and absorption coefficient α of the graphene depend on the voltage V_{Gate} applied to the layers and the resulting charge carrier density induced by the electrical field. Hence, a switchable optical absorption can be realized using this waveguide-integrated dual-graphene layer approach [6, 9].

2.2 Design of electrical network

The electrical connections surrounding the GP-EAM have been designed in order to facilitate an efficient interconnection to readily available radio frequency (RF) electronic components with 50 Ω impedance, that are widely used in data and telecommunications.

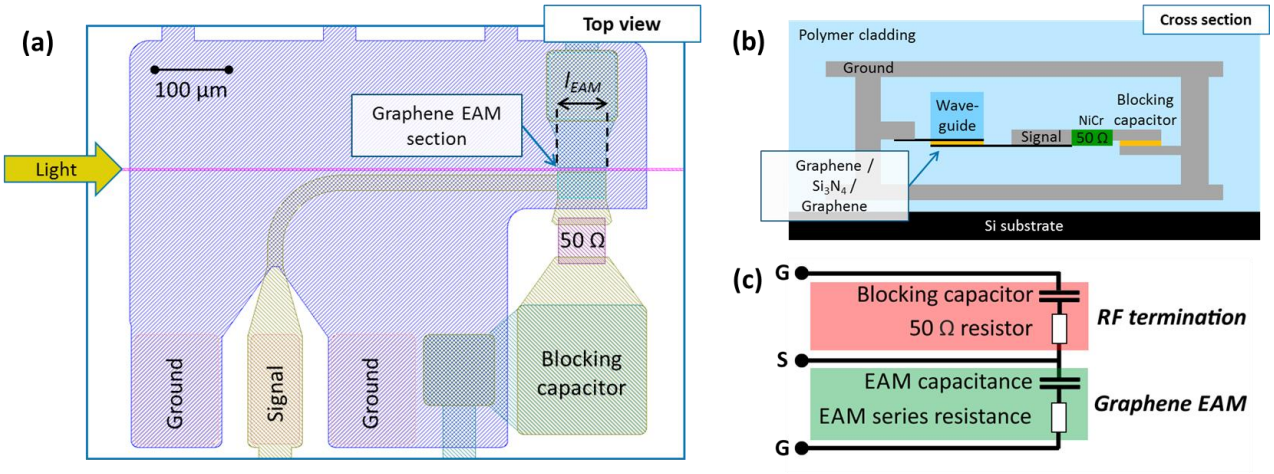

Figure 2. Top view (a) and cross section (b) (not to scale) of the 50 Ω impedance matched electrical pads and transmission lines as well as the 50 Ω termination and blocking capacitor integrated with the lumped element graphene EAM. (c) shows the equivalent circuit model of the device.

Figure 2 (a) shows the top view of the GP-EAM including the electrical layout. The electrical signal is fed into the structure via a co-planar ground-signal-ground pad configuration, while the RF waveguide is realized as a stripline. The stripline width is 23.7 µm and it consists of 30 nm Ti/200 nm Au/40 nm Ti. It is shielded by two ground planes (30 nm Ti/120 nm Au/40 nm Ti), which are connected by VIAs filled with gold, as can be seen from the cross section in Figure 2 (b). The spacing between the stripline and each ground plane is 20 µm, resulting in a total thickness of 40 µm. Hence, the polymer cladding material of the optical waveguide is at the same time the dielectric material of the RF waveguide. Assuming a polymer dielectric constant of 3.2, the impedance of the stripline was matched to 50 Ω at an RF frequency of 10 GHz. The chosen stripline layout of the electrical transmission line is unaffected by the dielectric constants and potential losses of the materials outside the ground planes as well as their thicknesses. This is advantageous especially for large scale integration of GP-EAMs e.g. into Active Optical Printed Circuit Boards (AO-PCBs), as they can be optimized independently of the respective environment.

The GP-EAM is situated at the end of the RF transmission line, where the graphene capacitor section connects signal and ground electrical contacts on one side. On the other side a 50 Ω ohmic NiCr resistor acts as RF termination in order to avoid reflections of the electrical signal. This resistor is connected to the ground contact through a blocking capacitor with 50 pF capacitance, which allows for the application of a DC offset voltage to the GP-EAM section while transmitting RF voltage signals above ca. 1 GHz.

2.3 Calculation of optoelectronic bandwidth

As explained in section 1, the optoelectronic bandwidth f_{3dB} of graphene-based EAMs demonstrated so far was exclusively limited by the RC time constant. Considering a specific metal-graphene contact resistance ρ_C and specific graphene sheet resistance ρ_S, the contributions to the series resistance and series capacity of a GP-EAM as shown in Figures 1 and 2 are listed in Table 1.

Table 1. Contributions to series resistance and series capacitance in a GP-EAM.

Contact resistance R_C	$R_C = 2\rho_C / l_{EAM}$
Access sheet resistance R_{Access}	$R_{Access} = 2\rho_S d / l_{EAM}$
Inner sheet resistance R_{Inner}	$R_{Inner} = r\rho_S w_{EAM} / l_{EAM}$

Effective termination $R_{Term.,eff.}$ $\quad R_{Term.,eff.} = R_{Term.}R_{Source}/\left(R_{Term.}+R_{Source}\right)$

EAM capacitance C_{EAM} $\quad C_{EAM} = \varepsilon_0\varepsilon_{r,SiN}l_{EAM}w_{EAM}/t_{SiN}$

While the access sheet resistance scales directly with the graphene's specific sheet resistance ρ_s, the sheet resistance of the graphene layer parts forming the capacitor section is reduced by a factor $r < 1$. This is due the enhanced charge carrier density in this area in operation of the device as the non-zero voltages applied to the EAM section induce free carriers [12]. This scaling factor has been found to be approx. 0.5 in the devices investigated in this work by evaluation of transistor test structures under different gate voltages. Hence, the sheet resistance inside the active section is effectively halved under operation.

Assuming a GP EAM active section with a length of l_{EAM}, a width of w_{EAM}, a graphene access width d as well as a silicon nitride insulator with a thickness of t_{SiN}, we consider the RC constant of the GP-EAM active region without taking the 50 Ω impedance of the RF source and termination into account. In this case the bandwidth of the lumped element $f_{3dB,lumped}$ equals:

$$f_{3dB,lumped} = \frac{1}{2\pi\left(R_C + R_{Access} + R_{Inner}\right)C_{EAM}}$$

$$= \frac{t_{SiN}}{2\pi\left(2\rho_C + 2\rho_S d + r\rho_S w_{EAM}\right)\varepsilon_0\varepsilon_{r,SiN}w_{EAM}}. \quad (1)$$

Despite specific sheet and contact resistances that should be minimized, the bandwidth is dominated by the insulator between both graphene layers and their overlap. As the insulator material and its thickness determine the voltages required for the EAM operation [9], this is usually not a variable in the device design. The overlap of the layers however should be reduced to the minimum value possible, as the bandwidth depends on terms that scale with $1/w_{EAM}$ and $(1/w_{EAM})^2$, respectively.

Furthermore, from Equation (1) it can be seen that the bandwidth of the active section is independent of its length. This would imply that an arbitrarily high extinction ratio could be achieved without compromising the high-frequency operation of the device by increasing its length. However, in the operation of real-world RF-capable devices, the impedance of source and termination cannot be disregarded and need to be taken into account, yielding the bandwidth $f_{3dB,total}$:

$$f_{3dB,total} = \frac{1}{2\pi\left(R_C + R_{Access} + R_{Inner} + R_{Term.,eff.}\right)C_{EAM}}$$

$$= \frac{t_{SiN}}{2\pi\left(2\rho_C + 2\rho_S d + r\rho_S w_{EAM} + l_{EAM}R_{Term.,eff.}\right)\varepsilon_0\varepsilon_{r,SiN}w_{EAM}} \quad (2)$$

In contrast to Equation (1) the total bandwidth also depends on a term that scales with $1/l_{EAM}$. As the impedance for RF source and termination are 50 Ω the effective termination is usually fixed at 25 Ω. Hence, the capacitance C_{EAM} is the sole controllable quantity in order to reduce the termination-induced bandwidth limitation. Especially the EAM width w_{EAM} should be reduced to the minimal feasible values in order to facilitate high-speed operation of graphene-based EAMs.

3. FABRICATION AND MEASUREMENT

3.1 Wafer-level fabrication of graphene EAMs

The GP-EAMs studied in this work were fabricated on a 4" wafer using HHI's PolyBoard platform [4, 13]. The passive optical access waveguides consist of the ZPU12-RI material system by ChemOptics Inc. With refractive indices of the waveguide core and cladding material being 1.48 and 1.45, respectively, the 3.2 µm by 3.2 µm cross-section waveguides are designed to be single mode throughout the spectral range from the O band across to the L band.

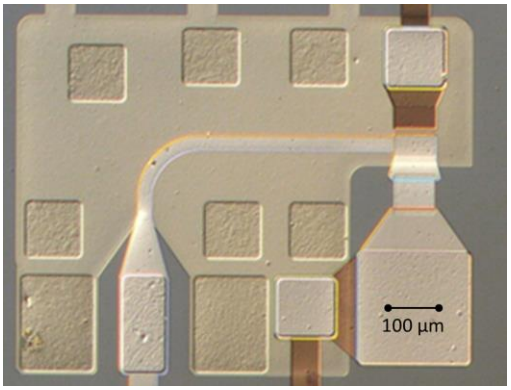

Figure 3. Micrograph of the top view of a fabricated GP-EAM before structuring of the passive polymer waveguide and deposition of the top electrical ground plate.

The polymer layers were fabricated by means of spin coating. The silicon nitride layers were applied by plasma-enhanced chemical vapor deposition and the metal structures by evaporation. The polymers, dielectrics and graphene layers were structured using reactive ion etching, while all metals involved were structured by wet etching. The up to 40 µm high VIAs between the electrical lower ground plate, the signal plane and the top ground plate where filled by galvanic reinforcement.

3.2 Dynamic characterization and GP-EAM bandwidth

The fabricated GP-EAMs were subject to dynamic large signal measurements relying on an Anritsu MP1763B pseudo-random-bit-stream (PRBS) generator and a Keysight DCA-X 86100D sampling oscilloscope. The complete system was capable of generating PRBS at data rates between 0.5 Gbit/s and 10 Gbit/s.

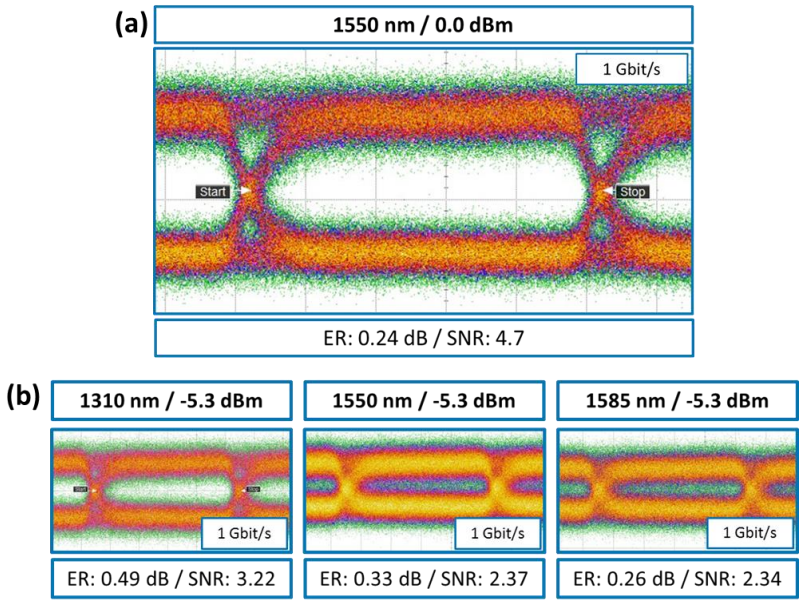

Figure 4. Eye diagram measurements at a data rate of 1 Gbit/s on a 100 µm long GP-EAM at 3.9 V_{pp} and a DC bias offset of +2 V. (a) shows the eye diagram at 1550 nm with a received power of 0.0 dBm. (b) shows the eye diagrams at a received power of -5.3 dBm for wavelengths of 1310 nm, 1550 nm and 1585 nm, respectively.

The eye diagram at a wavelength of 1550 nm for a 100 µm long GP-EAM fabricated as described above at a data rate of 1 Gbit/s and received optical power of 0.0 dBm is shown in Figure 4 (a). At 3.9 V_{pp} and a DC offset bias of 2.0 V a signal to noise ratio (SNR) of 4.7 was extracted. The 3dB-bandwidth of this device is 1.7 GHz. Although the extinction ratio of 0.24 dB is low, the eye is clearly open and does not exhibit any patterning. This is due to the pure RC limitation of the bandwidth in the GP-EAM.

For graphene, a low wavelength-dependence of the electro-optic properties is expected from theory with almost constant absorption between 400 nm and 2000 nm [14]. Hence, light of all wavelengths in between that is properly guided in the access waveguides should be modulated in the same GP-EAM with similar results. Figure 4 (b) shows the eye diagrams at the same operating point as above for a wavelength of 1310 nm (O band), 1550 nm (C band) and 1585 nm (L band). As the maximum available optical power was limited across this large wavelength span, the received power was set to -5.3 dBm for all cases in order to ensure better comparability. Although ER and SNR decrease slightly with increasing wavelength, the bandwidth and the RC characteristics are constant.

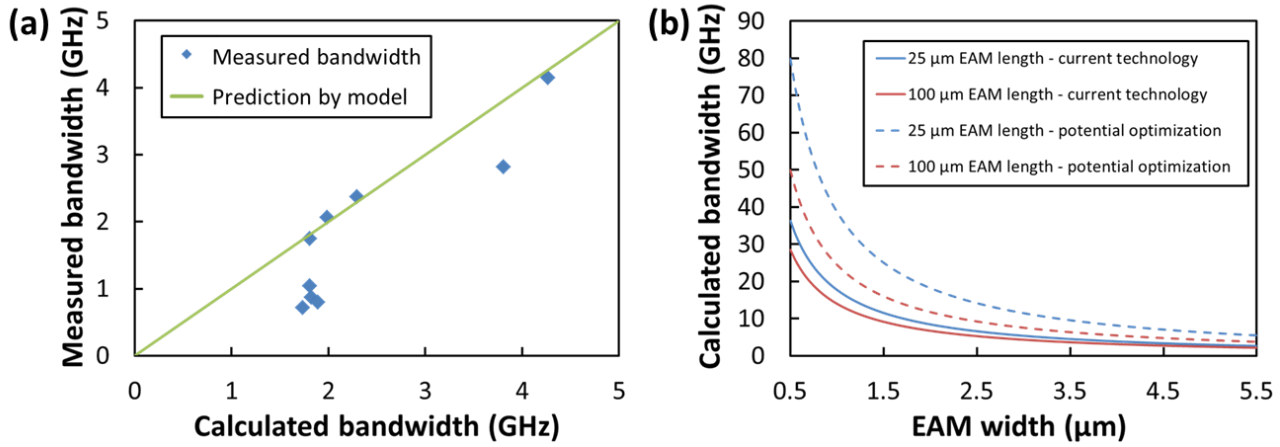

Figure 5. The measured optoelectronic bandwidth of GP-EAMs plotted over the bandwidth as predicted from Equation (2) is shown in (a). (b) shows the predicted bandwidths for 25 µm and 100 µm long GP-EAMs for the current graphene transfer technology and after potential process optimizations.

The bandwidth was determined for several GP-EAMs fabricated on the same PolyBoard wafer with bandwidths ranging between 0.7 GHz and 4.2 GHz, depending on the geometric parameters of the devices. Based on the Equation (2), the bandwidth was calculated assuming a graphene sheet resistance of ρ_S = 680 Ω/□, a contact resistance of ρ_C = 2700 Ω·µm and a scaling factor r = 0.5. These values were acquired from transmission-length-method and transistor test structures on the same wafer. Figure 5 (a) shows a plot of the measured optoelectronic bandwidth over the values as predicted from the model. It can be seen that for half of the devices under consideration, measured and predicted bandwidth are almost identical, while the other devices deviate to lower bandwidths. These deviations are consistent with an increase of the sheet resistance to approx. 1600 Ω/□ for these devices and can hence be attributed to process variations of the graphene layer transfer.

The current GP-EAMs featured EAM widths between 3.2 µm and 5.0 µm. From Equation (2) we can infer that the EAM width has a great influence on the achievable device bandwidth. In Figure 5 (b) the predicted bandwidth is plotted as a function of w_{EAM} for r = 0.5, t_{SiN} = 50 nm and d = 0.5 µm. The solid lines correspond to contact and sheet resistances as given above resulting from the current graphene transfer technology. Assuming an EAM width of 1.0 µm, bandwidths of 18 GHz and 14 GHz are predicted for EAM lengths of 25 µm and 100 µm, respectively. Considering potential process optimizations resulting in reasonable reductions of the sheet resistance to 400 Ω/□ and of the contact resistance to 1000 Ω·µm, bandwidths of 39 GHz and 24 GHz can be expected. By further decreasing the EAM width below 1 µm bandwidths well in excess of 50 GHz are possible for graphene-based EAMs.

4. CONCLUSION AND OUTLOOK

In this work we presented graphene-based electro-absorption modulators integrated in passive polymer waveguide networks of the PolyBoard platform. These were fabricated on a 4” wafer scale and characterized with dynamic measurements at a data rate of 1 Gbit/s at several wavelengths across the O, C and L band. The extracted optoelectronic bandwidths range between 0.7 GHz and 4.2 GHz depending on the geometric properties of the respective devices. The analytical model of the bandwidth devised for the graphene-based EAMs matches well with the measurements and predicts possible bandwidths of 24 GHz for new device iterations considering the current graphene transfer process. For

reduced graphene contact and sheet resistances and low EAM widths, bandwidths well in excess of 50 GHz can be expected from theory.

The demonstrated modulation bandwidths, the almost wavelength-independent properties as well as the seamless and cost-effective large-scale integration into low-index contrast waveguides make GP-EAM a very promising candidate for future data and telecommunications devices. A possible co-integration with already demonstrated graphene-based photodetectors [15] in the same fabrication process is especially promising for the realization of novel Active Optical Circuit Boards for High Performance Computing. The low temperature sensitivity of graphene-based optoelectronics [10] enables the uncooled operation inside polymer waveguides on large-area PCB-compatible substrates [16]. In this way the E/O and O/E conversion could be hidden from the user as in Active Optical Cables, greatly increasing the acceptance of optical connections in now electronics-dominated environments.

ACKNOWLEDGEMENTS

This work was partially funded by the European Commission [EU H2020 project HAMLET] and the German Federal Ministry of Education and Research [BMBF project Phonograph].

REFERENCES

[1] Smit, M., Leijtens, X., Ambrosius, H., Bente, E., van der Tol, J., Smalbrugge, B., Vries, T. de, Geluk, E.-J., Bolk, J., van Veldhoven, R., Augustin, L., Thijs, P., D'Agostino, D., Rabbani, H., Lawniczuk, K., Stopinski, S., Tahvili, S., Corradi, A., Kleijn, E., Dzibrou, D., Felicetti, M., Bitincka, E., Moskalenko, V., Zhao, J., Santos, R., Gilardi, G., Yao, W., Williams, K., Stabile, P., Kuindersma, P., Pello, J., Bhat, S., Jiao, Y., Heiss, D., Roelkens, G., Wale, M., Firth, P., Soares, F., Grote, N., Schell, M., Debregeas, H., Achouche, M., Gentner, J.-L., Bakker, A., Korthorst, T., Gallagher, D., Dabbs, A., Melloni, A., Morichetti, F., Melati, D., Wonfor, A., Penty, R., Broeke, R., Musk, B. and Robbins, D., "An introduction to InP-based generic integration technology," Semicond. Sci. Technol. 29(8), 83001 (2014).

[2] Lim, A. E.-J., Song, J., Fang, Q., Li, C., Tu, X., Duan, N., Chen, K. K., Tern, R. P.-C. and Liow, T.-Y., "Review of Silicon Photonics Foundry Efforts," IEEE J. Select. Topics Quantum Electron. 20(4), 405–416 (2014).

[3] Wörhoff, K., Heideman, R. G., Leinse, A. and Hoekman, M., "TriPleX: A versatile dielectric photonic platform," Advanced Optical Technologies 4(2), 189–207 (2015).

[4] Kleinert, M., Zhang, Z., Felipe, D. d., Zawadzki, C., Maese Novo, A., Brinker, W., Möhrle, M. and Keil, N., "Recent progress in InP/polymer-based devices for telecom and data center applications," Proc. SPIE 9365, 93650R (2015).

[5] Liu, M., Yin, X., Ulin-Avila, E., Geng, B., Zentgraf, T., Ju, L., Wang, F. and Zhang, X., "A graphene-based broadband optical modulator," Nature 474(7349), 64–67 (2011).

[6] Liu, M., Yin, X. and Zhang, X., "Double-layer graphene optical modulator," Nano letters 12(3), 1482–1485 (2012).

[7] Mohsin, M., Schall, D., Otto, M., Noculak, A., Neumaier, D. and Kurz, H., "Graphene based low insertion loss electroabsorption modulator on SOI waveguide," Opt. Express 22(12), 15292–15297 (2014).

[8] Phare, C. T., Daniel Lee, Y.-H., Cardenas, J. and Lipson, M., "Graphene electro-optic modulator with 30 GHz bandwidth," Nature Photon. 9(8), 511–514 (2015).

[9] Kleinert, M., Herziger, F., Reinke, P., Zawadzki, C., Felipe, D. d., Brinker, W., Bach, H.-G., Keil, N., Maultzsch, J. and Schell, M., "Graphene-based electro-absorption modulator integrated in a passive polymer waveguide platform," Opt. Mater. Express 6(6), 1800 (2016).

[10] Dalir, H., Xia, Y., Wang, Y. and Zhang, X., "Athermal Broadband Graphene Optical Modulator with 35 GHz Speed," ACS Photonics 3(9), 1564–1568 (2016).

[11] Shaforost, O., Wang, K., Goniszewski, S., Adabi, M., Guo, Z., Hanham, S., Gallop, J., Hao, L. and Klein, N., "Contact-free sheet resistance determination of large area graphene layers by an open dielectric loaded microwave cavity," J. Appl. Phys. 117(2), 24501 (2015).

[12] Castro Neto, A. H., Guinea, F., Peres, N. M. R., Novoselov, K. S. and Geim, A. K., "The electronic properties of graphene," Rev. Mod. Phys. 81(1), 109–162 (2009).

[13] Felipe, D. d., Kleinert, M., Zawadzki, C., Polatynski, A., Irmscher, G., Brinker, W., Moehrle, M., Bach, H.-G., Keil, N. and Schell, M., "Recent Developments in Polymer-Based Photonic Components for Disruptive Capacity Upgrade in Data Centers," J. Lightwave Technol., pp(99), 1 (2016).
[14] Mak, K. F., Ju, L., Wang, F. and Heinz, T. F., "Optical spectroscopy of graphene. From the far infrared to the ultraviolet," Solid State Communications 152(15), 1341–1349 (2012).
[15] Gan, X., Shiue, R.-J., Gao, Y., Meric, I., Heinz, T. F., Shepard, K., Hone, J., Assefa, S. and Englund, D., "Chip-integrated ultrafast graphene photodetector with high responsivity," Nature Photon. 7(11), 883–887 (2013).
[16] Dangel, R., Hofrichter, J., Horst, F., Jubin, D., La Porta, A., Meier, N., Soganci, I. M., Weiss, J. and Offrein, B. J., "Polymer waveguides for electro-optical integration in data centers and high-performance computers," Optics express 23(4), 4736–4750 (2015).